Unoccupied aerial system enabled functional modeling of maize (*Zea mays* L.) height reveals dynamic expression of loci associated to temporal growth.

Steven L. Anderson II[1,#a], Seth C. Murray[1,*], Yuanyuan Chen[1,#b], Lonesome Malambo[2], Anjin Chang[3], Sorin Popescu[2], Dale Cope[4], and Jinha Jung[3,#c]

[1]Department of Soil and Crop Sciences, Texas A&M University, College Station, TX 77843.

[2]Department of Ecosystem Science and Management, Texas A&M University, College Station, TX, 77843.

[3]School of Engineering and Computer Sciences, Texas A&M University - Corpus Christi, Corpus Christi, TX 78412

[4]Department of Mechanical Engineering, Texas A&M University, College Station, TX 77843.

[#a]Current Address: Department of Environmental Horticulture, University of Florida, Institute of Food and 12 Agricultural Sciences, Mid-Florida Research and Education Center, Apopka, FL 32703.

[#b]Current Address: National Key Laboratory of Crop Genetic Improvement, Huazhong Agricultural University, Hongshan District, Wuhan, 430070, China.

[#c]Current Address: Department of Civil Engineering, Purdue University, West Lafayette, IN 47907.

[*]Corresponding Author

Email: sethmurray@tamu.edu

Conflicts of interest

The authors declare no conflict of interest associated with the work described in this manuscript.

Abstract

Unoccupied aerial systems (UAS) were used to phenotype growth trajectories of inbred maize populations under field conditions. Three recombinant inbred line populations were surveyed on a weekly basis collecting RGB images across two irrigation regimens (irrigated and non-irrigated/rain fed). Plant height, estimated by the 95th percentile (P95) height from UAS generated 3D point clouds, exceeded 70% correlation to manual ground truth measurements and 51% of experimental variance was explained by genetics. The Weibull sigmoidal function accurately modeled plant growth (R^2: >99%; RMSE: < 4 cm) from P95 genetic means. The mean asymptote was strongly correlated (r^2=0.66-0.77) with terminal plant height. Maximum absolute growth rates (mm d^{-1}) were weakly correlated to height and flowering time. The average inflection point ranged from 57 to 60 days after sowing (DAS) and was correlated with flowering time (r^2=0.45-0.68). Functional growth parameters (asymptote, inflection point, growth rate) alone identified 34 genetic loci, each explaining 3 to 15% of total genetic variation. Plant height was estimated at one-day intervals to 85 DAS, identifying 58 unique temporal quantitative trait loci (QTL) locations. Genomic hotspots on chromosome 1 and 3 indicated chromosomal regions associated with functional growth trajectories influencing flowering time, growth rate, and terminal growth. Temporal QTL demonstrated unique dynamic expression patterns not observable previously, no QTL were significantly expressed throughout the entire growing season. UAS technologies improved phenotypic selection accuracy and permitted monitoring traits on a temporal scale previously infeasible using manual measurements, furthering understanding of crop development and biological trajectories.

Author summary

Unoccupied aerial systems (UAS) now can provide high throughput phenotyping to functionally model plant growth and explore genetic loci underlying temporal expression of dynamic phenotypes, specifically plant height. Efficient integration of temporal phenotyping via UAS, will improve the scientific understanding of dynamic, quantitative traits and developmental trajectories of important agronomic crops, leading to new understanding of plant biology. Here we present, for the first time, the dynamic nature of quantitative trait loci (QTL) over time under field conditions. To our knowledge, this is first empirical study to expand beyond selective developmental time points, evaluating functional and temporal QTL expression in maize (*Zea mays* L.) throughout a growing season within a field-based environment.

Introduction

Phenotypic characterization of agricultural plant populations has lagged in scale, density, and accuracy when compared with genomic data [1]. Due to resource demands of labor and time-sensitive components in conventional phenotyping, most manually measured traits are acquired at only one time point in the growing season and constrained in the number of samples. This creates a limited scope of biological understanding when associating genomic information with the underlying traits of interest through plant development [2]. Advances in technologies including computer vision, robotics, remote sensing, and unoccupied vehicles have facilitated the development of high-throughput phenotyping (HTP) platforms which can minimize phenotypic bottlenecks [3, 4].

Implementation of HTP systems provides the ability to collect temporal phenotypic measurements on large representative populations within field settings, to understand how

77 individuals interact with their environments [3, 5, 6]. Unoccupied aerial systems (UAS) are
78 especially useful to increase the size of populations and field studies investigated, collecting RGB
79 images, and reconstructing three dimensional representations of field crop trials using structure
80 from motion methodology [6-15]. UAS height estimates of maize have previously been validated
81 using correlations to traditional manual measurements and evidence of equivalent or greater
82 phenotypic variation partitioned to genetic factors [7, 9, 15, 16]. To our knowledge the majority
83 of reported field based phenotyping of maize with HTP platforms has focused on hybrid trials [6-
84 9, 15, 17-19] but, limited reports have been published on the evaluation of inbred trials [20-22],
85 specifically genetic mapping populations. Inbred lines in maize are substantially shorter and have
86 less biomass than hybrids, lacking heterosis.

87 Maize height is important as a physiological and a highly heritable agronomic trait [23-26]
88 commonly collected due to its ease of measurement, agronomic importance, and correlation to
89 hybrid grain yield in some environment and management scenarios [15, 27-32]. Manually
90 measured plant height is commonly collected after reproductive maturity as the distance from the
91 ground to the tip of the tassel, flag leaf, or peduncle. The genetic architecture of plant height in
92 maize has been determined to fit an infinitesimal model (i.e. very large numbers of small additive
93 effect loci) with some large effect loci likely fixed during domestication and early selection [23].
94 Functional genetic variation in terminal plant height has been shown to be controlled through
95 hormones; mutations within the (i) gibberellin biosynthesis pathways [33] and crosstalk with other
96 phytohormomes including: (ii) auxin [34] and (iii) brassinosteriods [35-38]. Hormones are well
97 known to fluctuate throughout plant growth, responding to environmental and developmental
98 stimuli [39-42]. Traditional QTL studies using phenotypic data at a single terminal (end of season)
99 time point can only represent accumulated effects, ignoring the dynamic nature of many

agronomically important traits which, like hormones, change and can be identified as functions of time [43]. To our knowledge, Wang, Zhang (20) is the only reported field based temporal association study in maize using UAS.

Plant height is an ideal phenotype to explore the temporal patterns of QTL expression in maize. Using UAS, we evaluated three recombinant inbred line (RIL) linkage mapping populations under field conditions and captured the dynamic growth patterns of plant height across these maize inbreds. The objectives of this study were to: (i) evaluate UAS procedures developed for hybrids to estimate heights within inbred maize populations; (ii) model and compare growth patterns across genetic populations; (iii) evaluate temporal patterns of QTL expression through the growing season, and (iv) evaluate the temporal expression patterns for previously reported QTL.

Results and Discussion

UAS surveys and image processing quality

A total of 18 and 11 flights were conducted over the bi-parental mapping populations using the DJI Phantom 3 Pro and Tuffwing UAV Mapper, respectively (S1 Table). Early season DJI Phantom 3 Pro data collection prior to 35 DAS resulted in limited to no plant structure reconstructed within the 3D point clouds, indicating that higher resolution imaging would be necessary to reconstruct early season plant structure. Out of 29 flights, 16 were observed to be of high quality while only eight flight dates (35, 43, 57, 62, 65, 69, 100, and 117 DAS) conformed to statistical quality tests (S1 File) and were used for the remainder of this study (Fig 1; S2 Table).

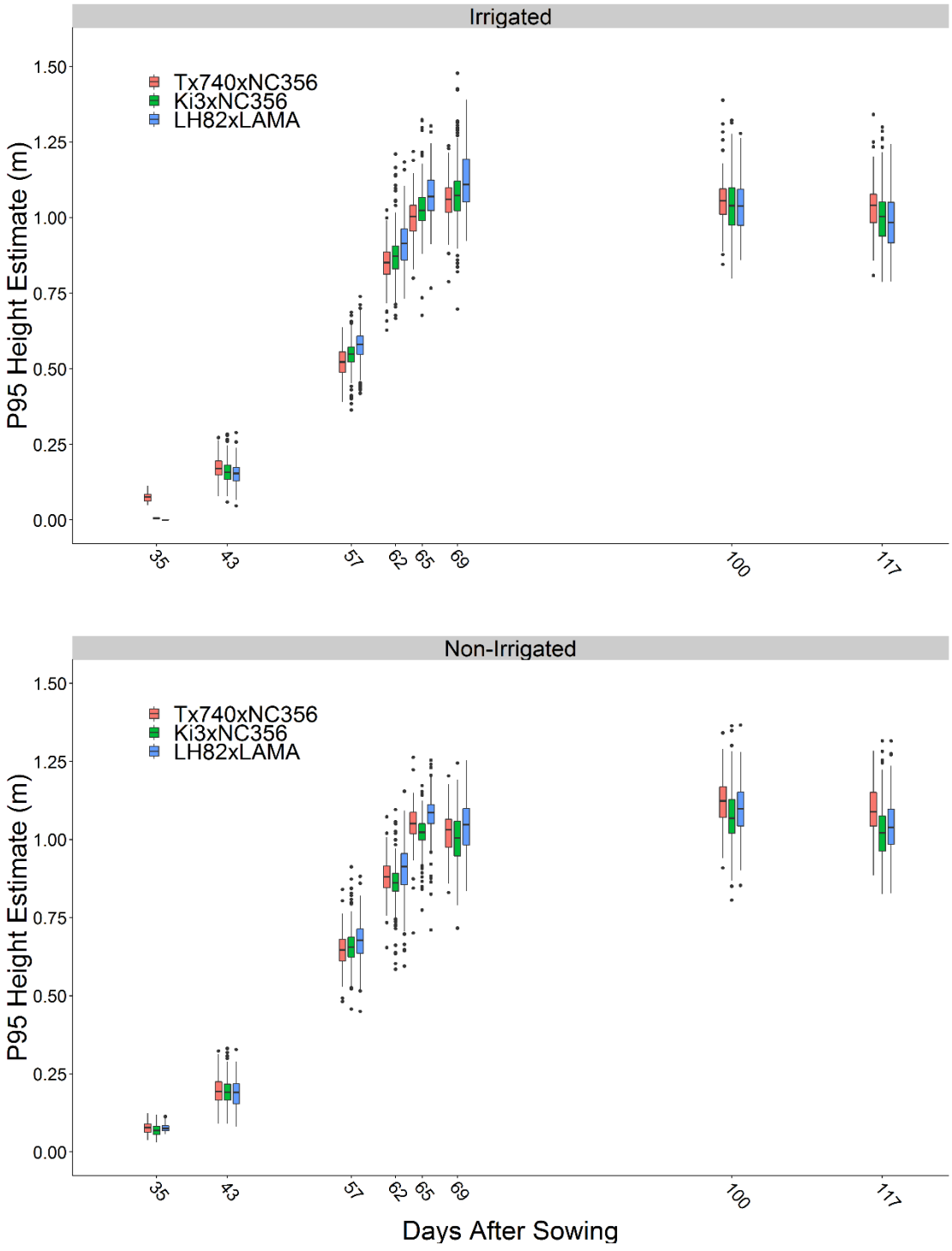

Fig 1. UAS P95 height estimates summarized by flight date. Although the three populations were genetically diverse, the mean growth patterns behaved similarly. Little differentiation could be seen early in the season between genotypes, where the measurement error may have been smaller that genotypic differences, as the plants reached their peak height and flowered, height differences became much greater.

Genetic variance decomposition

Variance component decomposition demonstrated total phenotypic variance increased throughout the growing season for all inbred populations (Fig 2, black circles), as has been found in hybrid trials [7, 15]. UAS phenotypic variance for height did not exceed manual, terminal plant height (PHT_{TRML}, Fig 2 M bar). Genetic variance averaged 51% (excluding 35 DAS) over the season fluctuating from flight to flight, but generally increasing until reaching a terminal height plateau. The proportion of variance attributed to genetics of

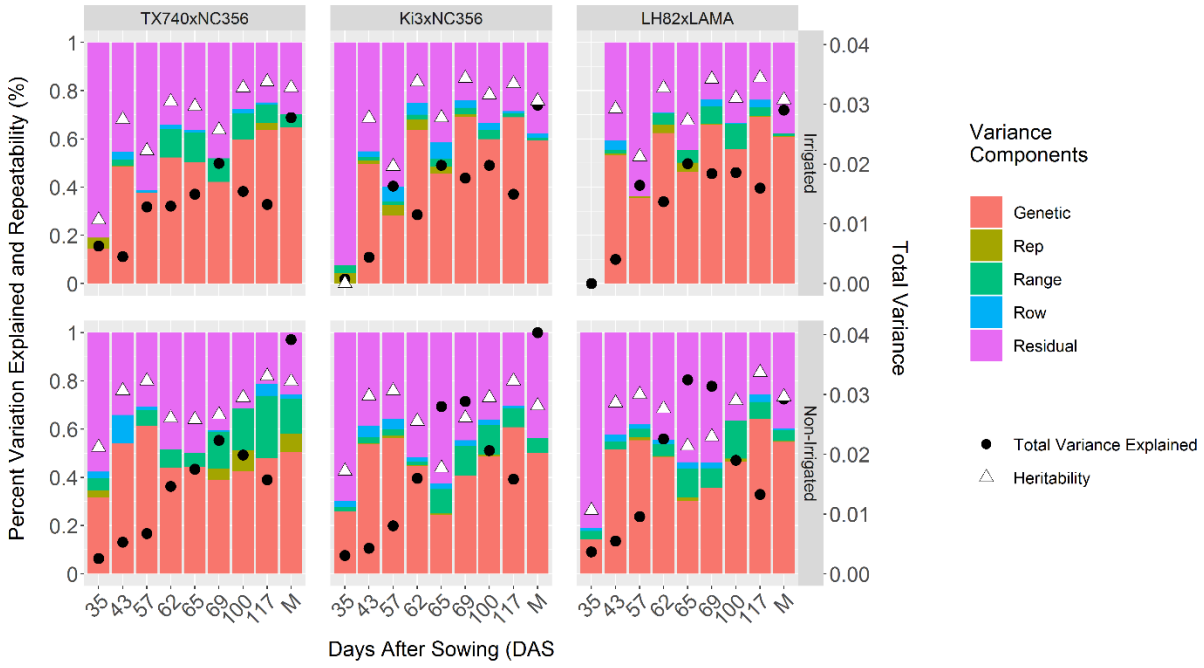

Fig 2. Variance component decomposition of UAS P95 height estimates. The percent variation explained in the model of Eq. 1 for individual UAS surveys of three RIL populations showed that genetic and residual (error) variation, were the main drivers of variability observed. Total variance (black circles) increased as the plants grew over later flight dates and was higher for manual (M) than UAS measurements. That the percent variance measures and heritability were similar for M and UAS suggests that UAS compressed all variance sources similarly

144 plant height (PHT_{TRML}), as measured from the ground to the tip of the tassel, were numerically
145 greater (irrigated: 62 ± 3%; non-irrigated: 52 ± 3), but not statistically (α=0.05) different from
146 across UAS genetic variance.

147 **Sigmoidal modeling of UAS height estimates**

148 The Weibull function, a sigmoidal growth function, modeled maize inbred temporal growth
149 (mean R^2>0.99, RMSE ranging from 2.4 to 3.7 cm) across all populations and environment (Fig
150 3). Significant differences in asymptote, the maximum height, were only found between
151 Tx740xNC356 (1.10 m) and LH82xLAMA (1.08 m) with a 2 cm difference in means under
152 irrigation. LH82 [44] is the earliest to flower and shortest of the inbred lines adaptable to these
153 environments and had among the lowest asymptote and inflection point, but moderate growth rate.
154 In comparison, PHT_{TMRL} was significantly different across populations (1.66, 1.59, and
155 1.57 m) under irrigated conditions for Tx740xNC356, Ki3xNC356, and LH82xLAMA,
156 respectively. The reduced means of the asymptote demonstrate the inherent biases of UAS
157 estimation of plant height compared with manual measurements [8, 12, 13, 15]; ~0.5 m
158 underestimate of height has been documented in past studies of hybrid maize at flight altitudes of
159 120 m [15]. The average difference in height estimates increased by ~5 and ~10 cm when
160 compared to P99 and P100 point cloud estimates, indicating that the reduction was not caused
161 solely by the lower percentile, P95. The combination of flight altitude and reduced plant canopy
162 density of the inbreds likely biased the UAS towards shorter estimates. Biases aside, numerical
163 rankings between asymptote and PHT_{TRML} were correctly consistent in ranking Tx740xNC356,
164 Ki3xNC356, and LH82xLAMA population means from tallest to shortest and Pearson correlations
165 (r) (Irrigated: 0.77, 0.74, and 0.74; Non-Irrigated: 0.66, 0.72, and 0.74; S1-S3 Fig)

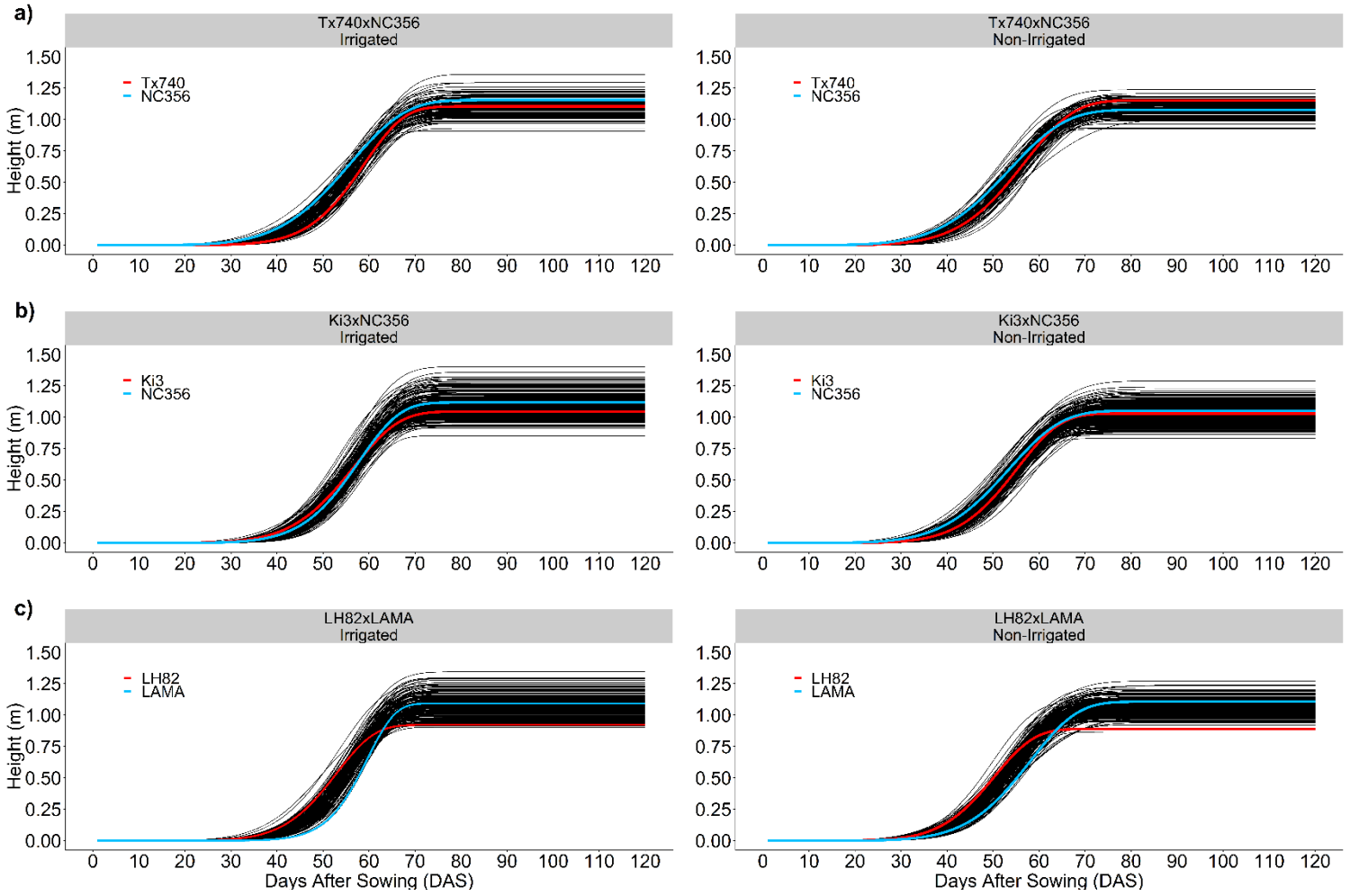

Fig 3. Nonlinear Weibull functional modeling of growth trajectories. Sigmoidal curves based off the Weibull function (Eq. [3]) effectively modeled the growth of each entry. For each population the female parent (red line) and the male parent (blue line) crossed over demonstrating that early season height was not predictable by standard manual terminal height measurements.

170 indicated highly significant (α=0.05), positive linear correlations between UAS asymptotes
171 estimates and PHT_{TRML} measurements.

172 The inflection point of the Weibull model is biologically important to identify the DAS in
173 which maximum AGR is occurring; this point has been shown to be highly correlated to flowering
174 time in hybrid trials [15]. Significant differences were found between each population's mean for
175 inflection point (58.6, 58.0, and 57.5 d for Tx740xNC356, Ki3xNC356, and LH82xLAMA) within
176 the irrigated trial (Fig 4c). Abiotic stress related to water limitations in non-irrigated trials delayed
177 the inflection point by two days on average across the populations. Inflection point had low
178 positive correlations to PHT_{TRML} (Irrigated: 0.30, 0.27, and 0.34; Non-Irrigated: 0.02, 0.22, and
179 0.24; S1-S3 Fig) but high correlations to flowering time (DTA/DTS) (Irrigated: 0.60/0.45,
180 0.59/0.58, and 0.64/0.59; Non-Irrigated: 0.61/0.56, 0.55/0.53, and 0.68/0.66; S1-S3 Fig). PHT P95
181 estimates were negatively correlated (r= -0.74:-0.50) to inflection points during the early season
182 but gradually progressed toward a positive correlation ~10 days after the mean inflection point
183 (S1-S3 Fig). Later inflection points had extended vegetative growth periods leading to taller plants,
184 indicating the possibility of pleiotropic QTL for both flowering time and growth rate across the
185 functional curve parameters. Because correlation was high but imperfect, tall genotypes with
186 earlier inflection points could indicate better fitness in stressful environments, as these plants reach
187 their terminal height quickly without regard to environmental stresses.

188 The growth rate parameter, influencing the steepness of the Weibull curve, significantly differed
189 (α=0.05) in its means across the populations in both environments (Irrigated: 6.9, 7.6, and 8.2;
190 Non-irrigated: 6.3, 6.5, and 6.8). The first derivative of the Weibull function (Eq. 4), the absolute
191 growth rate (AGR), calculated at the inflection point ($x=x_0$) equals the maximum AGR. The
192 maximum AGR occurred ~50-60 DAS, which was shortly before flowering, in this period

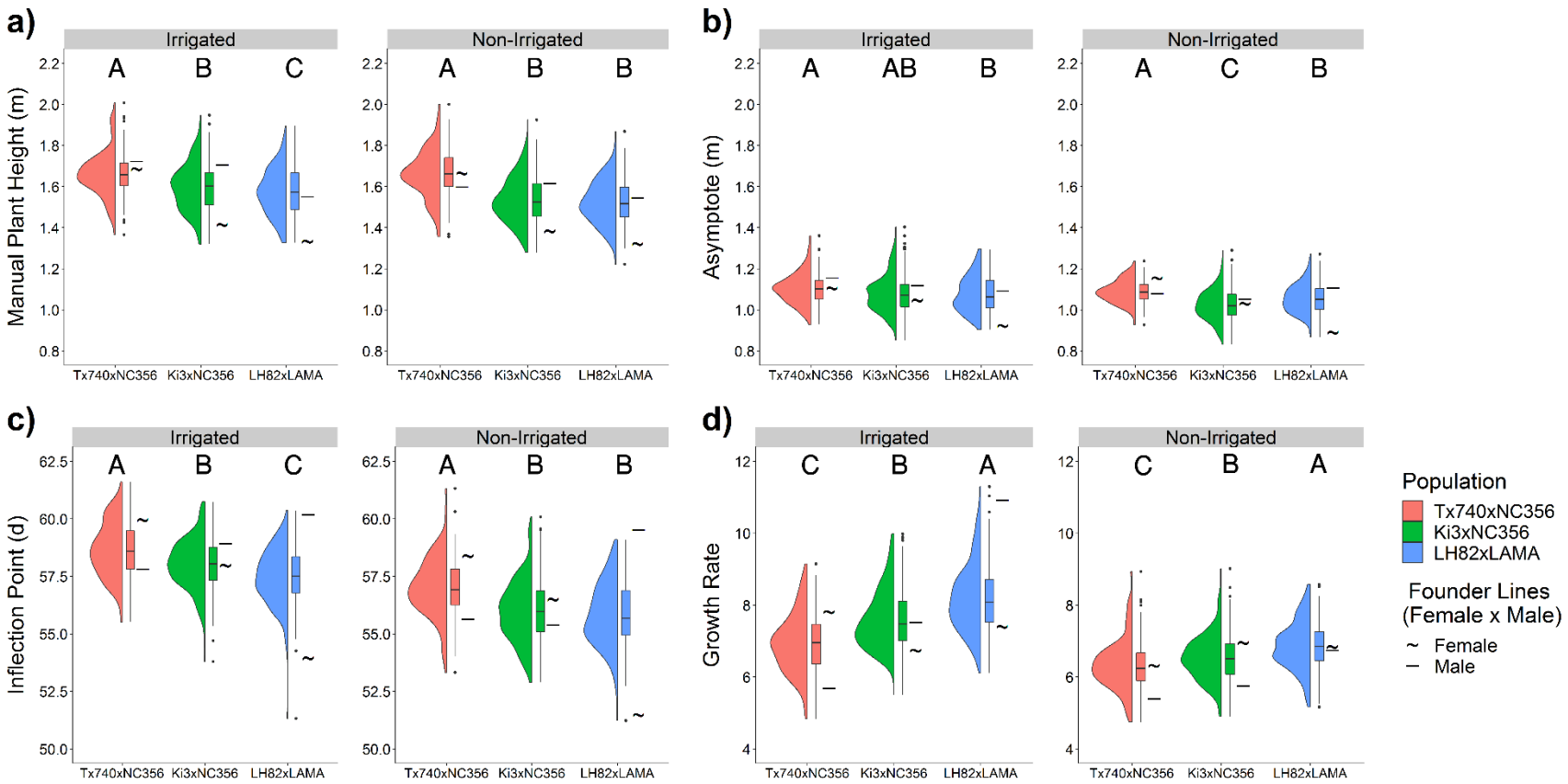

Fig 4. Distribution of Weibull functional parameters. Entry BLUPS of **[a]** manual terminal plant height, **[b]** Weibull asymptote, **[c]** Weibull inflection point, and **[d]** Weibull growth rate for each mapping population demonstrated variability both within and between these populations with substantial transgressive segregation in most cases. Letters above define significant differences in means at α=0.05.

cells are both dividing and elongating within the internodes above the ear node [45-47]. Significant differences were found in the maximum AGR across populations within the irrigated trial (48, 52, and 56 mm d^{-1}) and LH82xLAMA was 3 mm d^{-1} greater than the other populations in the non-irrigated trial despite being the shortest population overall. A reduction in AGR was observed within the non-irrigated trial (4, 7, and 8 mm d^{-1} Tx740xNC356, Ki3xNC356, and LH82xLAMA, respectively) likely due to water stress during this period [48]. Overall this demonstrated that the AGR had heritable genetic diversity and was phenotypically plastic in response to different environmental conditions.

QTL mapping

Manual terminal height associations. Nine QTL were identified for PHTTRML across the three populations and two environments (S3 Table) each explaining 5.1 to 9.4% of genetic variance. All PHTTRML associations had additive effects of ~3 cm (S3 Table). One region was identified across two populations q1_172 (LH82xLAMA; irrigated) and q1_176 (Tx740xNC356; non-irrigated), localizing to the 280 to 284 Mbs region of chromosome 1. We identified a single genomic region, 98 to 128 Mbs on chromosome 2 that co-localized within the same genetic background (Ki3xNC356) across different environmental treatments (q2_70 irrigated and q2_69 non-irrigated). The limited co-localization of QTLs across bi-parental populations is part of the difficulty of identifying genomic regions that can be utilized in genetic backgrounds beyond those in which they were discovered [49, 50]. This also demonstrated the lack of statistical power in the smaller of the three populations Tx740xNC356 (n=110). It has been empirically shown that population size is the most critical factor in QTL linkage mapping [24].

Functional parameter associations. UAS estimates in modeling temporal growth of maize can identify dynamic QTL [51]. Analysis of QTLs using the three functional parameters of the

223 Weibull curve as phenotypes identified 13, 9, and 12 significant marker associations with the
224 asymptote, growth rate, and inflection point, respectively (S5 Table). Asymptote QTLs explained
225 genetic variation ranging from 3.4% to 14.3% with additive effects ranging from 2 to 5 cm,
226 consistent with PHTTRML. High correlations between asymptote and PHTTRML indicated that
227 similar QTL would likely be detected using both traits. Two PHTTRML QTLs, q1_172
228 LH82xLAMA (irrigated) and q1_176 Tx740xNC356 (non-irrigated), co-localized with an
229 asymptote QTL, q1_173 of LH82xLAMA (irrigated) (Fig 5; S3 Table). Additional co-
230 localizations were found between q6_67 Tx740xNC356 (irrigated) asymptote and q6_62
231 Ki3xNC356 (irrigated) PHTTRML, as well as, q8_10 LH82xLAMA (non-irrigated) asymptote
232 with q8_14 Ki3xNC356 (irrigated) PHTTRML and q8_12 Ki3xNC356 (non-irrigated)
233 PHTTRML.

234 The seven growth rate QTL each explained 5.6 to 15% of the genotypic variance with
235 additive effects ranging from 0.2 to 0.3 DAS^{-1} (S5 Table). Inflection point QTL each explained 4.3
236 to 13% of the genotypic variance with additive effects ranging from 0.2 to 0.5 d (S5 Table).
237 Irrigated Ki3xNC356 trial *q*4_61 and irrigated LH82xLAMA *q*1_173/*q*1_176 were associated
238 with inflection point and asymptote, while non-irrigated LH82xLAMA *q*10_20 was associated
239 with inflection point and growth rate (S5 Table). The co-localization of QTL associated with
240 multiple parameters of the sigmoidal growth function indicated these regions more than others
241 may have an effect on defining the overall developmental trajectory of maize height. The limited
242 number of co-localizations demonstrates these traits are both genetically variable and highly
243 plastic with the environment.

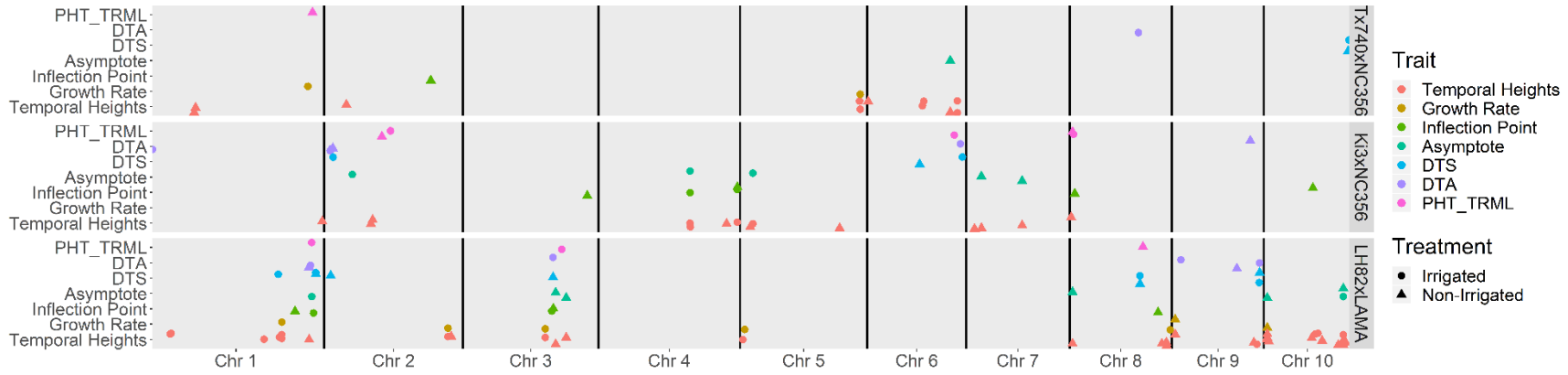

244

245 **Fig 5. Col-localization of agronomic and functional growth QTL associations.** Significant QTL co-localized across agronomic
246 traits (PHT_TRML: Manual, terminal plant height; DTA: Days to anthesis; DTS: Days to silking), functional growth parameters
247 (asymptote, inflection point, growth rate) and temporal height estimates from the Weibull curves. Temporal expression of all height
248 QTL can be visualized in **S4 Fig**.

249 Multiple QTL were identified within the LH82xLAMA trials for PHT_{TRML}, asymptote,
250 inflection point, and flowering time (DTA/DTS; S4 Table) within the 273 to 287 Mbs region of
251 chromosome 1 and the 140 to 176 Mbs region of chromosome 3 (Fig 5). The QTL region of
252 chromosome 3 harbors ZmMADS69 (GRMZM2G171650; Chr3: 158979321..159007265), a
253 regulator of flowering time with pleiotropic effects on plant height. ZmMADS69 has higher
254 expression levels in temperate compared to tropical germplasm, leading to significant detection in
255 temperate by tropical crosses [52], such as LH82xLAMA among others
256 [23, 24, 53]. The identified region on chromosome 1 contained the viviparous8 (vp8;
257 GRMZM2G010353; Chr1: 286390345..286398537) locus which exhibits dwarfism due to reduced
258 cell proliferation [54]. Both loci may be deterministic QTL (dQTL) because the differential allelic
259 variation affected the whole growth process [55] and was unaffected by environmental stimuli;
260 ZmMADS69 effect was not influenced by day length [52] and vp8 exhibited normal plant
261 hormone response [54]. These results coupled with basic biological understanding indicated that
262 allelic changes in loci can have a fundamental impacts on the functional growth trajectory of maize,
263 in contrast to the small shift in phenotypic expression of a single trait It is therefore understandable
264 that these two "major genes" have been previously identified and described in multiple studies,
265 while the smaller and ephemeral effect loci are mostly unknown.
266
267 **Temporal QTL expression**. In addition to detecting QTL for the three parameters of the
268 Weibull function, 58 QTL were also detected using individuals' daily heights from 20 to 85 DAS
269 predicted using the Weibull function. Between 4 and 20 unique QTLs were identified, based on
270 peak position (Fig 5; S6 Table). Comparison of mean physical distance of the flanking markers
271 for each the 58 unique QTLs demonstrated 23 QTLs were within 1 Mbp of a plant height

candidate gene and an additional 18 QTL were less than 5 Mbp from a candidate gene. Most of the 58 unique QTLs demonstrated a very dynamic nature of QTL affecting plant height throughout the growing season. For example, q5_119 in the irrigated Tx740xNC356 trial, was detected from 22 to 62 DAS explaining 21% of the genetic variation at 54 DAS (Fig 6a; S6 Table). In comparison, q5_35 of irrigated Tx740xNC356 trial was detected from 66 to 74 DAS explaining 11% of the genetic variation at 67 DAS (Fig 6a). Temporal QTL expression was different for each population across environmental treatments (i.e. irrigation) demonstrating differential genomic localization while maintaining similarities in temporal expression. Specifically, within the Tx740xNC356 population, both irrigation regimens (i.e. environments) have a temporally broad QTL (q5_119 irrigated and q2_55 non- irrigated) prior to inflection point (~58 DAS), followed by QTLs detected at shorter temporal intervals after the inflection point and may relate to the elongation of specific internode groupings [45-47]. Additionally, trends in QTL temporal expression between populations exhibited unique temporal expression patterns. For example, Tx740xNC356 exhibited QTLs prior to the inflection point at early growth stages, whereas Ki3xNC356 exhibited no detectable QTLs until ~50 DAS. Low phenotypic variation could be the cause, as could, greater numbers of smaller effect loci, towards an infinitesimal model, that would also be hard to detect.

Identified QTLs demonstrated dynamic trends in additive phenotypic effects (Fig 6, right side). In general, these results show that the additive effects found at the peak significance DAS of a temporal QTL is a result of the cumulative effect of a gradual increase in the effect size of each genomic region (Fig 6). QTLs with peak expression early within the season had significantly smaller additive effect estimates than at later points in the growing season; due to reduced overall variation across individuals in the population at early growth stages (e.g. Fig 6b

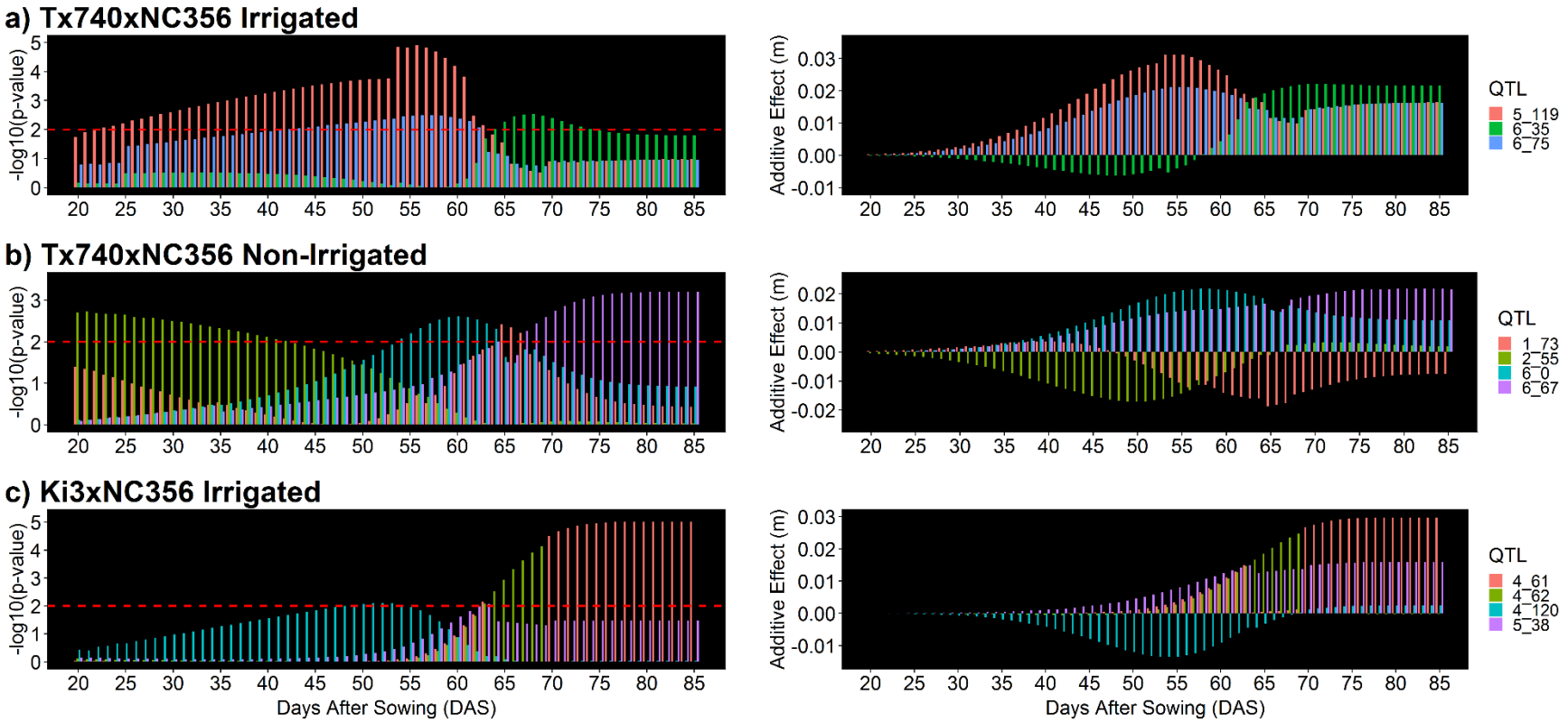

Fig 6. Visualization of temporal trends in QTL expression. Temporal trends in QTL expression were observed in all QTL across populations and environments. Most QTL were under the significance threshold (left side) of LOD=2 (red dashed line) at some point during the growing season; however the smaller additive effects (right side) during these periods would not have been expected to be declared a QTL.

302 *q*2_55). Some QTL effects (Fig 6b *q*6_0) also appeared to lose their association throughout
303 season, however it is likely due to their effects statistically being diluted by new QTL that
304 become significant (Fig 6b *q*6_67). While most individual QTL maintained their directional
305 effect (Fig 6a; q5_119 and *q*6_75), some surprisingly switched effect directions within the
306 growing season (q6_35). Understanding the biological basis of this switching phenomena would
307 be both interesting and important for optimizing plant growth. Caution should be used to
308 interpret all of these QTL as loci that functionally affect height and plant growth rather than
309 height QTL per se; loci affecting rooting, plant health or photoperiod sensitivity all could impact
310 plant measured height.

311 Analysis across the entire linkage map demonstrated that directional changes in additive
312 effect size were present during the growing season (S4 and S5 Fig). Within marker assisted
313 selection protocols, targeting consistent directional effects may result in greater gains than those
314 of temporal bi-directional effects. Before additional work is conducted temporal effect size should
315 first be validated through near isogenic lines across genetic backgrounds or in heterogeneous
316 inbred families [56]. However, we speculate that the temporal trend of the effect size, like many
317 QTL effects remains dependent on the genetic background, abiotic, and biotic interactions
318 experienced in each environment, and this G x E interaction. If temporal shifts in directional effect
319 are valid and not due to over inflations via false positives and limited population size; statistical
320 models accounting for directional effect shifts will be necessary to incorporate temporal datasets
321 of dynamic, quantitative traits within prediction modeling approaches to plant breeding, such as
322 genomic selection.

323

324

Materials and methods

Germplasm material and experimental design

Three bi-parental mapping populations were developed from breeding lines segregating for loci discovered in an earlier genome wide association study [28, 57] of hybrids for height and grain yield. The recombinant inbred line (RIL) progeny were derived from the crosses of Tx740xNC356 (tropical/tropical; 110 RILs), Ki3xNC356 (tropical/tropical; 239 RILs) and LH82xLAMA-YC (temperate/tropical; 178 RILs). Tx740 (LAMA2002-12-1-B-B-B) [58] is a parent in the "LAMA" inbred line (pedigree [((LAMA2002-12-1-B-B-B-B/LAMA2002-1-5-B-B-B-B)-3-2-B-1-B3-B]) and these two lines would be expected to share 50% of their genome. In 2018, the mapping populations were planted in a randomized complete block design (RCBD) with two replications across two environments (irrigated and non-irrigated) having dimensions of 0.76 m row spacing, and 3.81 m plot lengths.

Unoccupied aerial system image collection

Two platforms were used, a rotary wing and a fixed wing UAV, to collect RGB data. For the rotary wing, a DJI Phantom 3 Professional with a 12-megapixel DJI FC300X camera was flown at an altitude of 25 m with to 80% forward and side image overlap. Fixed wing images were collected using a Tuffwing UAV Mapper (http://www.tuffwing.com) equipped with a 24-megapixel Sony a6000 RGB camera. Fixed wing surveys were conducted at a 120 m altitude with 80% image overlap. A total of 19 DJI Phantom 3 Professional flights were conducted throughout the growing season, while 11 Tuffwing UAV Mapper flights (starting 05/17/2018) were conducted after early season to mechanical setbacks of the Tuffwing (S2 Table). After QC/QA, a total of 16 flights were used for height estimates based on quality of the processed orthomosaic images.

All of the Tuffwing flights were processed in Agisoft PhotoScan [59], while the majority of the DJI Phantom flights were processed in Pix4Dmapper [60], based on collaborators comfort and preference with the associated software. In general, these software packages are equivalent and used to identify common features (tie points) across images followed by triangulation and distortion adjustment optimization to generate densified 3D point clouds, DSM, and orthomosaic images. Height estimates were extracted from the three dimensional point clouds following the procedures of [15]. In short, the ground points were identified from the point cloud using the hierarchical robust interpolation algorithm within FUSION/LDV. Identified ground points were used to interpolate the digital elevation model, followed by subtracting the DEM from the original point cloud to produce the canopy surface model. The plot level polygon shapefiles were created using the R/UAStools::plotshpcreate [15] function in R and the 95th percentile height estimates were extracted for each experimental plot.

Statistical Inference

Variance component estimates and heritability. From the extracted canopy height metrics (P95), we fit mixed linear models utilizing residual maximum likelihood (REML) in JMP version 14.0.0 [61] to define best linear unbiased predictors (BLUPs) of the inbreds by their entry number. Models were fit on a per flight date basis. The individual mapping populations were evaluated as a randomized complete block design (RCBD, Eq. 1) including spatial regression (range and row [furrow irrigation runs down rows], this is called row and column, respectively, where furrow irrigation is not used).

$$Y = \mu + \sigma_G^2 + \sigma_r^2 + \sigma_i^2 + \sigma_j^2 + \sigma_\varepsilon^2 \quad (1)$$

with terms entry (σ_G^2), replicate (σ_r^2) range (σ_i^2), row (σ_j^2) and residual error (σ_ε^2).

Broad sense heritability (H^2) estimates were calculated on an entry means basis (Eq.2).

$$H^2 = \frac{\sigma_G^2}{\sigma_G^2 + \sigma_\varepsilon^2/\mathrm{r}} \quad (2)$$

Within each environment, H^2 estimates were calculated for each population separately while including replicates (r) for each of the UAS flight dates.

Nonlinear function. The three parameter Weibull sigmoid growth model (Eq. 3) was used to summarize the

$$f(x) = L\left(1 - e^{\left(-\left(x/x_0\right)^b\right)}\right) \quad (3)$$

height as a function of DAS (x) with the asymptote (L), inflection point (x_0), and the growth rate (b) of the fitted curve. The asymptote (L; m) is maximum value of the curve which represents maximum/terminal plant height (PHT_{TRML}). The inflection point (x_0; DAS) indicates the DAS where the slope of the logarithmic phase is at its absolute maximum. The growth rate (b) is an empirical constant which defines the shape of the curve and relates to the absolute growth rate (Eq. 4; m d^{-1}) when $x=x_0$. Sigmoidal curves were fit using the Fit Curve tool in JMP 14 and

$$\frac{\delta y}{\delta x}\left(L\left(1-e^{\left(-\left(x/x_0\right)^b\right)}\right)\right)=\frac{Lbe^{\left(-\left(x/x_0\right)^b\right)}\left(\frac{x}{x_0}\right)^b}{x} \quad (4)$$

parameters were estimated on an entry basis utilizing the extracted BLUPs or the individual environment REML models described above. Significance of the functional parameters were evaluated using the chi squared (X^2) test ($\alpha = 0.05$, df = 1) to identify logistical curves with poor fits to UAS height estimates, these were subsequently removed from future analysis. Using the associated Weibull functional parameters, height estimates were imputed on one day intervals (1 to 85 DAS) for each inbred entry in their associated environments.

Genotyping and linkage map construction

The genotyping was described in Chen, Murray (62), and is paraphrased here. Genotype samples were collected from $F_{3:4}$ seedlings grown under greenhouse conditions, where eight samples were bulked per genotype. The CTAB method [63] was used to extract DNA and samples were sent to AgReliant Genetics LLC, where they were genotyped by Infinium® assays for 17,444 single nucleotide polymorphisms (SNPs). The linkage groups and physical locations were provided with the SNP chip of which 716 markers locations were unknown or withheld due to intellectual property rights, resulting in 17,019 SNPs with known reference locations (B73 RefGEN_v3).

Individuals with >10% missing values and SNPs with >10% missing values were dropped from the data set resulting in 5316, 5628, and 6231 polymorphic SNPs for the Ki3/NC356, Tx740/NC356, and LH82/LAMA populations, respectively. Crosspoints were predicted using the

crosspoint subcommand of SNPbinner [64] to clean data set of double recombinants. The emission probability was set to 0.9 (-p 0.9), the continuous genotype region was set to 0.1% (-r 0.001) of the chromosome size, and the transition probability was calculated using a crosscount of 7,500,000 (-c 7,500,000). The visualize subcommand was used to evaluate the efficiency of the calculated break points to the original SNP calls and identify satisfactory crosspoint parameters. The crosspoint output identified break point locations for each RIL and the prediction of genotypic homogeneity of each region between breakpoint and the SNP calls were adjusted accordingly. Marker datasets filtered by SNPbinner were constructed into linkage maps using the MAP function of QTL IciMapping version 4.1.0.0 (http://www.isbreeding.net/) software. Redundant markers were identified using the "BIN" functionality and redundant markers with greater missing data rate were excluded. Linkage groups were defined by "By Anchor Only" setting and the marker orders were defined by their physical locations using the "By Input" ordering algorithm. Recombination frequencies between markers were calculated based on F_3 marker frequencies by denoting the "POP.ID" to eight.

The final genetic maps consisted of 1530, 2571, and 2324 SNPs after removal of redundant markers. The genetic map distances were calculated in QTL IcIMappering using the Kosambi mapping function, and the total map lengths were estimated to be 1315, 1207, and 1474 cM for the Tx740xNC356, Ki3xNC356, and LH82xLAMA populations, respectively.

Linkage Mapping

The entries phenotyped in 2018 were advanced several generations following initial DNA extraction at $F_{3:4}$ and were evaluated in the field at F_6 generation or greater. For this reason, heterozygous calls (1) were set to missing (-1) and QTL analysis was performed assuming RIL genotype frequencies ("POP.ID" = 4). Analysis by other methods (e.g. treating as F_3) were also

436 tested to ensure conclusions were similar, but detection power was much lower, likely due to the
437 software trying to fit dominance effects expected to be rare or absent by the F_6 generation.
438 Inclusive Composite Interval Mapping [65] of Additive (ICIM-ADD) QTL was conducted in the
439 QTL IciMapping v4.1 using the BIP (QTL mapping for bi-parental populations) function. The step
440 parameter was set to 1.0 cM and the probability of inclusion in the stepwise regression (PIN) was
441 set to 0.001. The focus of this study was on understanding the temporal shifts in the marker trait
442 associations of plant height, rather than identifying regions of high confidence that could be used
443 in later marker assisted selection. For these reasons, we defined QTL of interest liberally as those
444 with LOD > 2.0 and percent variation explained ≥ 3% [66], however LOD and other metrics are
445 provided to extract more conservative thresholds. Using the imputed heights from 1 to 85 DAS,
446 ICIM-ADD was performed on each DAS, for each population in each environment separately to
447 access the temporal shifts in allelic effects and marker–trait associations.

448 A list of candidate genes was obtained from Wallace, Zhang (25). In short, candidate genes
449 were identified from (i) literature, (ii) mining the MaizeGDB database for known height mutants,
450 and (iii) searching the maize genome annotation on Phytozome genes annotated with “auxin”,
451 “brassinosteroid” and/or “gibberellin”. Distance for the center of the QTL confidence interval to
452 nearest candidate gene with the same chromosome were identified.

453 **Data Availibility**

454 All of the raw and processed data relevant to this study is publically available on Dryad
455 Digital Repository (68). All raw and processed image output files from this study are publicly
456 available and can be obtained by request to the authors.

Acknowledgements

The authors would like to acknowledge Misty Miles and all members of the Texas A&M UAS project. David Rooney, Jacob Pekar and Stephen Labar for their agronomic and technical support. Graduate students and undergraduate/high school employees for their hard work and effort maintaining fields and collecting phenotypic data. Special thank you to AgReliant Genetics, LLC. and Dr. Ivan D. Barrero Farfan for funding and conducting the genotyping for this research. This project was made possible by financial support from USDA-NIFA-AFRI Award No. 2017-67013-26185 USDA-NIFA Hatch funds Texas A&M AgriLife Research the Texas Corn Producers Board the Iowa Corn Promotion Boardthe Eugene Butler Endowed Chair in Biotechnology and the Texas A&M College of Agriculture and Life Sciences Tom Slick Senior Graduate Fellowship.

Author contributions:

S.L.A. conceptualization, data curation, formal analysis, investigation, methodology, original draft, review and editing (lead), supervision, validation, visualization; S.C.M. conceptualization, funding acquisition, methodology, project administration, supervision, resources, review and editing (supporting); Y.C. data curation, methodology, review and editing (supporting);L.M. data curation, formal analysis, investigation, methodology, review and editing (supporting), software; S.P. conceptualization, funding acquisition, resources, review and editing (supporting), software, supervision; D.C.: conceptualization, funding acquisition, resources, review and editing (supporting), supervision; A.C. data curation, formal analysis, investigation, methodology, review and editing (supporting), software; J.J. data curation, formal analysis, investigation, methodology, resources, review and editing (supporting), software, supervision; I.D.B.F.: data curation, resources, funding acquisition, review and editing (supporting).

References

1. Pauli D, Chapman SC, Bart R, Topp CN, Lawrence-Dill CJ, Poland J, et al. The quest for understanding phenotypic variation via integrated approaches in the field environment. Plant Physiology. 2016;172(2):622-34.
2. Furbank RT, Tester M. Phenomics–technologies to relieve the phenotyping bottleneck. Trends in Plant Science. 2011;16(12):635-44.
3. Araus JL, Cairns JE. Field high-throughput phenotyping: the new crop breeding frontier. Trends in Plant Science. 2014;19(1):52-61.
4. Araus JL, Kefauver SC, Zaman-Allah M, Olsen MS, Cairns JE. Translating high-throughput phenotyping into genetic gain. Trends in Plant Science. 2018;23(5):451-66. doi: 10.1016/j.tplants.2018.02.001.
5. Sankaran S, Khot LR, Espinoza CZ, Jarolmasjed S, Sathuvalli VR, Vandemark GJ, et al. Low-altitude, high-resolution aerial imaging systems for row and field crop phenotyping: A review. European Journal of Agronomy. 2015;70:112-23.
6. Shi Y, Thomasson JA, Murray SC, Pugh NA, Rooney WL, Shafian S, et al. Unmanned aerial vehicles for high-throughput phenotyping and agronomic research. PloS One. 2016;11(7):e0159781.
7. Pugh N, Horne DW, Murray SC, Carvalho G, Malambo L, Jung J, et al. Temporal estimates of crop growth in sorghum and maize breeding enabled by unmanned aerial systems. The Plant Phenome Journal. 2018;1(1).
8. Malambo L, Popescu S, Murray S, Putman E, Pugh N, Horne D, et al. Multitemporal field-based plant height estimation using 3D point clouds generated from small unmanned aerial systems high-resolution imagery. International Journal of Applied Earth Observation and Geoinformation. 2018;64:31-42.
9. Chu T, Starek MJ, Brewer MJ, Murray SC, Pruter LS. Characterizing canopy height with UAS structure-from-motion photogrammetry—results analysis of a maize field trial with respect to multiple factors. Remote Sensing Letters. 2018;9(8):753-62.
10. Bendig J, Bolten A, Bennertz S, Broscheit J, Eichfuss S, Bareth G. Estimating biomass of barley using crop surface models (CSMs) derived from UAV-based RGB imaging. Remote Sensing. 2014;6(11):10395-412.
11. De Souza CHW, Lamparelli RAC, Rocha JV, Magalhães PSG. Height estimation of sugarcane using an unmanned aerial system (UAS) based on structure from motion (SfM) point clouds. International Journal of Remote Sensing. 2017;38(8-10):2218-30.
12. Holman FH, Riche AB, Michalski A, Castle M, Wooster MJ, Hawkesford MJ. High throughput field phenotyping of wheat plant height and growth rate in field plot trials using UAV based remote sensing. Remote Sensing. 2016;8(12):1031.
13. Watanabe K, Guo W, Arai K, Takanashi H, Kajiya-Kanegae H, Kobayashi M, et al. High-throughput phenotyping of sorghum plant height using an unmanned aerial vehicle and its application to genomic prediction modeling. Frontiers in Plant Science. 2017;8.
14. Chang A, Jung J, Maeda MM, Landivar J. Crop height monitoring with digital imagery from unmanned aerial system (UAS). Computers and Electronics in Agriculture. 2017;141:232-7.

15. Anderson SL, Murray S, Malambo L, Ratcliff C, Popescu S, Cope D, et al. Prediction of maize grain yield before maturity using improved temporal height estimates of unmanned aerial systems. The Plant Phenome Journal. 2019;2. doi: 10.2135/tppj2019.02.0004.
16. Anthony D, Elbaum S, Lorenz A, Detweiler C, editors. On crop height estimation with UAVs. Intelligent Robots and Systems (IROS 2014), 2014 IEEE/RSJ International Conference on; 2014: IEEE.
17. Li W, Niu Z, Chen H, Li D, Wu M, Zhao W. Remote estimation of canopy height and aboveground biomass of maize using high-resolution stereo images from a low-cost unmanned aerial vehicle system. Ecological Indicators. 2016;67:637-48.
18. Varela S, Assefa Y, Prasad PV, Peralta NR, Griffin TW, Sharda A, et al. Spatio-temporal evaluation of plant height in corn via unmanned aerial systems. Journal of Applied Remote Sensing. 2017;11(3):036013.
19. Geipel J, Link J, Claupein W. Combined spectral and spatial modeling of corn yield based on aerial images and crop surface models acquired with an unmanned aircraft system. Remote Sensing. 2014;6(11):10335-55.
20. Wang X, Zhang R, Song W, Han L, Liu X, Sun X, et al. Dynamic plant height QTL revealed in maize through remote sensing phenotyping using a high-throughput unmanned aerial vehicle (UAV). Scientific Reports. 2019;9(1):3458.
21. Han L, Yang G, Yang H, Xu B, Li Z, Yang X. Clustering field-based maize phenotyping of plant-height growth and canopy spectral dynamics using a UAV remote-sensing approach. Frontiers in Plant Science. 2018;9:1638.
22. Han L, Yang G, Dai H, Xu B, Yang H, Feng H, et al. Modeling maize above-ground biomass based on machine learning approaches using UAV remote-sensing data. Plant Methods. 2019;15(1):10.
23. Peiffer JA, Romay MC, Gore MA, Flint-Garcia SA, Zhang Z, Millard MJ, et al. The genetic architecture of maize height. Genetics. 2014;196(4):1337-56.
24. Anderson SL, Mahan AL, Murray SC, Klein PE. Four parent maize (FPM) population: Effects of mating designs on linkage disequilibrium and mapping quantitative traits. The Plant Genome. 2018;11. doi: 10.3835/plantgenome2017.11.0102.
25. Wallace JG, Zhang X, Beyene Y, Semagn K, Olsen M, Prasanna BM, et al. Genome-wide association for plant height and flowering time across 15 tropical maize populations under managed drought stress and well-watered conditions in Sub-Saharan Africa. Crop Science. 2016;56(5):2365-78.
26. Li X, Zhou Z, Ding J, Wu Y, Zhou B, Wang R, et al. Combined linkage and association mapping reveals QTL and candidate genes for plant and ear height in maize. Frontiers in Plant Science. 2016;7:833.
27. Farfan IDB, Murray SC, Labar S, Pietsch D. A multi-environment trial analysis shows slight grain yield improvement in Texas commercial maize. Field Crops Research. 2013;149:167-76.
28. Chen Y. High-density linkage map construction, mapping of agronomic traits in tropical maize (Zea Mays L.) and validating SNPs controlling maize grain yield and plant height in southern hybrid testcrosses. Doctoral dissertation.: Texas A&M University. Available electronically from http : / /hdl .handle .net /1969 .1 /158620.; 2016.
29. Katsvairo TW, Cox WJ, Van Es HM. Spatial growth and nitrogen uptake variability of corn at two nitrogen levels. Agronomy Journal. 2003;95(4):1000-11.

30. Machado S, Bynum E, Archer T, Lascano R, Wilson L, Bordovsky J, et al. Spatial and temporal variability of corn growth and grain yield. Crop Science. 2002;42(5):1564-76.
31. Mallarino A, Oyarzabal E, Hinz P. Interpreting within-field relationships between crop yields and soil and plant variables using factor analysis. Precision Agriculture. 1999;1(1):15-25.
32. Yin X, McClure MA, Jaja N, Tyler DD, Hayes RM. In-season prediction of corn yield using plant height under major production systems. Agronomy Journal. 2011;103(3):923-9.
33. Lawit SJ, Wych HM, Xu D, Kundu S, Tomes DT. Maize DELLA proteins dwarf plant8 and dwarf plant9 as modulators of plant development. Plant and Cell Physiology. 2010;51(11):1854-68.
34. Multani DS, Briggs SP, Chamberlin MA, Blakeslee JJ, Murphy AS, Johal GS. Loss of an MDR transporter in compact stalks of maize br2 and sorghum dw3 mutants. Science. 2003;302(5642):81-4.
35. Hartwig T, Chuck GS, Fujioka S, Klempien A, Weizbauer R, Potluri DPV, et al. Brassinosteroid control of sex determination in maize. Proceedings of the National Academy of Sciences. 2011;108(49):19814-9.
36. Winkler RG, Helentjaris T. The maize Dwarf3 gene encodes a cytochrome P450-mediated early step in Gibberellin biosynthesis. The Plant Cell. 1995;7(8):1307-17.
37. Makarevitch I, Thompson A, Muehlbauer GJ, Springer NM. Brd1 gene in maize encodes a brassinosteroid C-6 oxidase. PloS One. 2012;7(1):e30798.
38. Wang Y, Zhao J, Lu W, Deng D. Gibberellin in plant height control: old player, new story. Plant Cell Reports. 2017;36(3):1-8.
39. Ferreira FJ, Kieber JJ. Cytokinin signaling. Current opinion in plant biology. 2005;8(5):518-25.
40. Finkelstein RR. Studies of abscisic acid perception finally flower. The Plant Cell. 2006;18(4):786-91.
41. Huq E. Degradation of negative regulators: a common theme in hormone and light signaling networks? Trends in plant science. 2006;11(1):4-7.
42. Lorenzo O, Solano R. Molecular players regulating the jasmonate signalling network. Current opinion in plant biology. 2005;8(5):532-40.
43. Wu R, Lin M. Functional mapping—how to map and study the genetic architecture of dynamic complex traits. Nature Reviews Genetics. 2006;7(3):229.
44. Holden's Foundation Seeds I, inventorCorn 'LH82' patent 008500037. 1985.
45. Fournier C, Andrieu B. Dynamics of the elongation of internodes in maize (Zea mays L.): analysis of phases of elongation and their relationships to phytomer development. Annals of Botany. 2000;86(3):551-63.
46. Morrison T, Kessler J, Buxton D. Maize internode elongation patterns. Crop Science. 1994;34(4):1055-60.
47. Robertson M. Relationships between internode elongation, plant height and leaf appearance in maize. Field Crops Research. 1994;38(3):135-45.
48. Tardieu F, Reymond M, Muller B, Granier C, Simonneau T, Sadok W, et al. Linking physiological and genetic analyses of the control of leaf growth under changing environmental conditions. Australian Journal of Agricultural Research. 2005;56(9):937-46.
49. Beavis W. QTL analyses: power, precision, and accuracy, ‖ in: Molecular analysis of complex traits.(Paterson, AH ed.). CRC Press, Cleveland, USA; 1998.
50. Jannink J-L, Bink MC, Jansen RC. Using complex plant pedigrees to map valuable genes. Trends in plant science. 2001;6(8):337-42.

612 51. Wu R, Lin M. Functional mapping—how to map and study the genetic architecture of
613 dynamic complex traits. Nature Reviews Genetics. 2006;7(3):229-37.
614 52. Liang Y, Liu Q, Wang X, Huang C, Xu G, Hey S, et al. Zm MADS 69 functions as a
615 flowering activator through the ZmRap2. 7 - ZCN 8 regulatory module and contributes to
616 maize flowering time adaptation. New Phytologist. 2019;221(4):2335-47.
617 53. Hirsch CN, Foerster JM, Johnson JM, Sekhon RS, Muttoni G, Vaillancourt B, et al. Insights
618 into the maize pan-genome and pan-transcriptome. The Plant Cell. 2014;26(1):121-35.
619 54. Lv H, Zheng J, Wang T, Fu J, Huai J, Min H, et al. The maize d2003, a novel allele of VP8,
620 is required for maize internode elongation. Plant Molecular Biology. 2014;84(3):243-57.
621 55. Wu R, Wang Z, Zhao W, Cheverud JM. A mechanistic model for genetic machinery of
622 ontogenetic growth. Genetics. 2004;168(4):2383-94.
623 56. Tuinstra M, Ejeta G, Goldsbrough P. Heterogeneous inbred family (HIF) analysis: a method
624 for developing near-isogenic lines that differ at quantitative trait loci. Theoretical and
625 Applied Genetics. 1997;95(5-6):1005-11.
626 57. Farfan IDB, Gerald N, Murray SC, Isakeit T, Huang P-C, Warburton M, et al. Genome wide
627 association study for drought, aflatoxin resistance, and important agronomic traits of maize
628 hybrids in the sub-tropics. PloS One. 2015;10(2):e0117737.
629 58. Mayfield K, Betrán FJ, Isakeit T, Odvody G, Murray SC, Rooney WL, et al. Registration of
630 maize germplasm lines Tx736, Tx739, and Tx740 for reducing preharvest aflatoxin
631 accumulation. Journal of Plant Registrations. 2012;6(1):88-94.
632 59. AgiSoft PhotoScan Professional. (Version 1.2.6) (Software). Retrieved from
633 http://wwwagisoftcom/downloads/installer/. 2016.
634 60. Pix4Dmapper. Pix4D SA. www.pix4d.com. 2018.
635 61. JMP®. Version 14.0.0. SAS Institute Inc, Cary, NC, 1989-2018. 2018.
636 62. Chen Y, Murray SC, Barrero ID, Kolomiets MV, Rooney WL, Wang F. Validating SNPs'
637 effects on maize grain yield and plant height in Txxas testcross hybrids. Molecular Breeding.
638 In Preparation.
639 63. Chen D-H, Ronald P. A rapid DNA minipreparation method suitable for AFLP and other
640 PCR applications. Plant Molecular Biology Reporter. 1999;17(1):53-7.
641 64. Gonda I, Ashrafi H, Lyon DA, Strickler SR, Hulse-Kemp AM, Ma Q, et al. Sequencing-
642 based bin map construction of a tomato mapping population, facilitating high-resolution
643 quantitative trait loci detection. The Plant Genome. 2018;12.
644 65. Li H, Ye G, Wang J. A modified algorithm for the improvement of composite interval
645 mapping. Genetics. 2007;175(1):361-74.
646 66. Li H, Ribaut J-M, Li Z, Wang J. Inclusive composite interval mapping (ICIM) for digenic
647 epistasis of quantitative traits in biparental populations. Theoretical and Applied Genetics.
648 2008;116(2):243-60.
649 67. Archontoulis SV, Miguez FE. Nonlinear regression models and applications in agricultural
650 research. Agronomy Journal. 2015;107(2):786-98.
651 68. Anderson SL, Murray SC, Chen Y, Malambo M, Chang A, Popescu S, Cope D, Jung J.
652 Unoccupied aerial system enabled functional modeling of maize (Zea mays L.) height
653 reveals dynamic expression of loci associated to temporal growth. Dryad Digital Repository.

Figures

Fig 1. UAS P95 height estimates summarized by flight date. Although the three populations were genetically diverse, the mean growth patterns behaved similarly. Little differentiation could be seen early in the season between genotypes, where the measurement error may have been smaller that genotypic differences, as the plants reached their peak height and flowered, height differences became much greater.

Fig 2. Variance component decomposition of UAS P95 height estimates. The percent variation explained in the model of Eq. 1 for individual UAS surveys of three RIL populations showed that genetic and residual (error) variation, were the main drivers of variability observed. Total variance (black circles) increased as the plants grew over later flight dates and was higher for manual (M) than UAS measurements. That the percent variance measures and heritability were similar for M and UAS suggests that UAS compressed all variance sources similarly

Fig 3. Nonlinear Weibull functional modeling of growth trajectories. Sigmoidal curves based off the Weibull function (Eq. [3]) effectively modeled the growth of each entry. For each population the female parent (red line) and the male parent (blue line) crossed over demonstrating that early season height was not predictable by standard manual terminal height measurements.

Fig 4. Distribution of Weibull functional parameters. Entry BLUPS of [a] manual terminal plant height, [b] Weibull asymptote, [c] Weibull inflection point, and [d] Weibull growth rate for each mapping population demonstrated variability both within and between these populations with substantial transgressive segregation in most cases. Letters above define significant differences in means at α=0.05.

Fig 5. Col-localization of agronomic and functional growth QTL associations. Significant QTL co-localized across agronomic traits (PHT_TRML: Manual, terminal plant height; DTA: Days to anthesis; DTS: Days to silking), functional growth parameters (asymptote, inflection point, growth rate) and temporal height estimates from the Weibull curves. Temporal expression of all height QTL can be visualized in S4 Fig.

Fig 6. Visualization of temporal trends in QTL expression. Temporal trends in QTL expression were observed in all QTL across populations and environments. Most QTL were under the significance threshold (left side) of LOD=2 (red dashed line) at some point during the growing season; however the smaller additive effects (right side) during these periods would not have been expected to be declared a QTL.

Supporting information

S1 Fig. Tx740xNC356 correlation heatmaps. Heat map comparing correlations between manual terminal plant height (PHT), flowering time (DTA/DTS), functional parameters (asymptote, growth rate, inflection point), and UAS P95 estimates by flight date for the Tx740xNC356 population under **[a]** irrigated and **[b]** non-irrigated watering regimens. Growth rate is an empirical constant of the Weibull function which defines the maximum absolute growth rate (m d^{-1}).

S2 Fig. Ki3xNC356 correlation heatmaps. Heat map comparing correlations between manual terminal plant height (PHT), flowering time (DTA/DTS), functional parameters (asymptote, growth rate, inflection point), and UAS P95 estimates by flight date for the Ki3xNC356 population under [a] irrigated and [b] non-irrigated watering regimens. Growth rate is an empirical constant of the Weibull function which defines the maximum absolute growth rate (m d-1).

S3 Fig. LH82xLAMA correlation heatmaps. Heat map comparing correlations between manual terminal plant height (PHT), flowering time (DTA/DTS), functional parameters (asymptote, growth rate, inflection point), and UAS P95 estimates by flight date for the LH82xLAMA population under [a] irrigated and [b] non-irrigated watering regimens. Growth rate is an empirical constant of the Weibull function which defines the maximum absolute growth rate (m d-1).

S4 Fig. Visual representation of temporal QTL. Significant temporal height QTL. Red indicates positive allelic effect estimates, blue indicates negative allelic effect estimates, and black indicate non-significant (NS) genomic regions. Lines represent each of 5316, 5628, and 6231 polymorphic SNPs for the Ki3/NC356, Tx740/NC356, and LH82/LAMA populations, respectively, across the genome (X-axis).

S5 Fig. Visual representation of temporal allele effect estimate. Visual representation of temporal single marker analysis of the Weibull imputed height estimates. Lines represent each of 5316, 5628, and 6231 polymorphic SNPs for the Ki3/NC356, Tx740/NC356, and LH82/LAMA populations, respectively, across the genome (X-axis).

S1 Table. Summary of 2018 UAS flight dates. Summary of 2018 UAS flight dates of the fields containing the Tx740xNC356, Ki3xNC356, and LH82xLAMA populations, including: days after sowing (DAS), the number of images captured, the number of calibrated images, spatial resolution of the mosaic image and mean errors of the GCP geo-referencing.

S2 Table. Descriptive statistics of UAS flight dates by population. Summary statistics of the entries for each population (Tx740xNC356, Ki3xNC356, and LH82xLAMA) across the six identified flight dates with high quality point clouds for the irrigated and non-irrigated trials.

S3 Table. Manual plant height QTL. Summary of QTL identified using manual terminal plant height as the associated phenotype. Physical locations (bp) based on B73 RefGen_3, AGPv3.

S4 Table. Flowering time QTL Summary of significant QTL for flowering time. Physical locations (bp) based on B73 RefGen_3, AGPv3.

733
734 **S5 Table. Function growth parameter QTL.** Summary of significant QTL for functional
735 parameters of the Weibull sigmoid function. Physical locations (bp) based on B73 RefGen_3,
736 AGPv3. Growth rate (GR) is an empirical constant of the Weibull function which defines the
737 maximum absolute growth rate (m d^{-1}).
738
739 **S6 Table. Temporal height QTL.** Summary of significant temporal QTL for height estimates
740 imputed from Weibull sigmoid curve at discrete time points (i.e. DAS where significant
741 associations were identified.). Physical locations (bp) based on B73 RefGen_3, AGPv3.
742
743 **S1 File. Statistical methods to identify flight to remove from temporal dataset.**

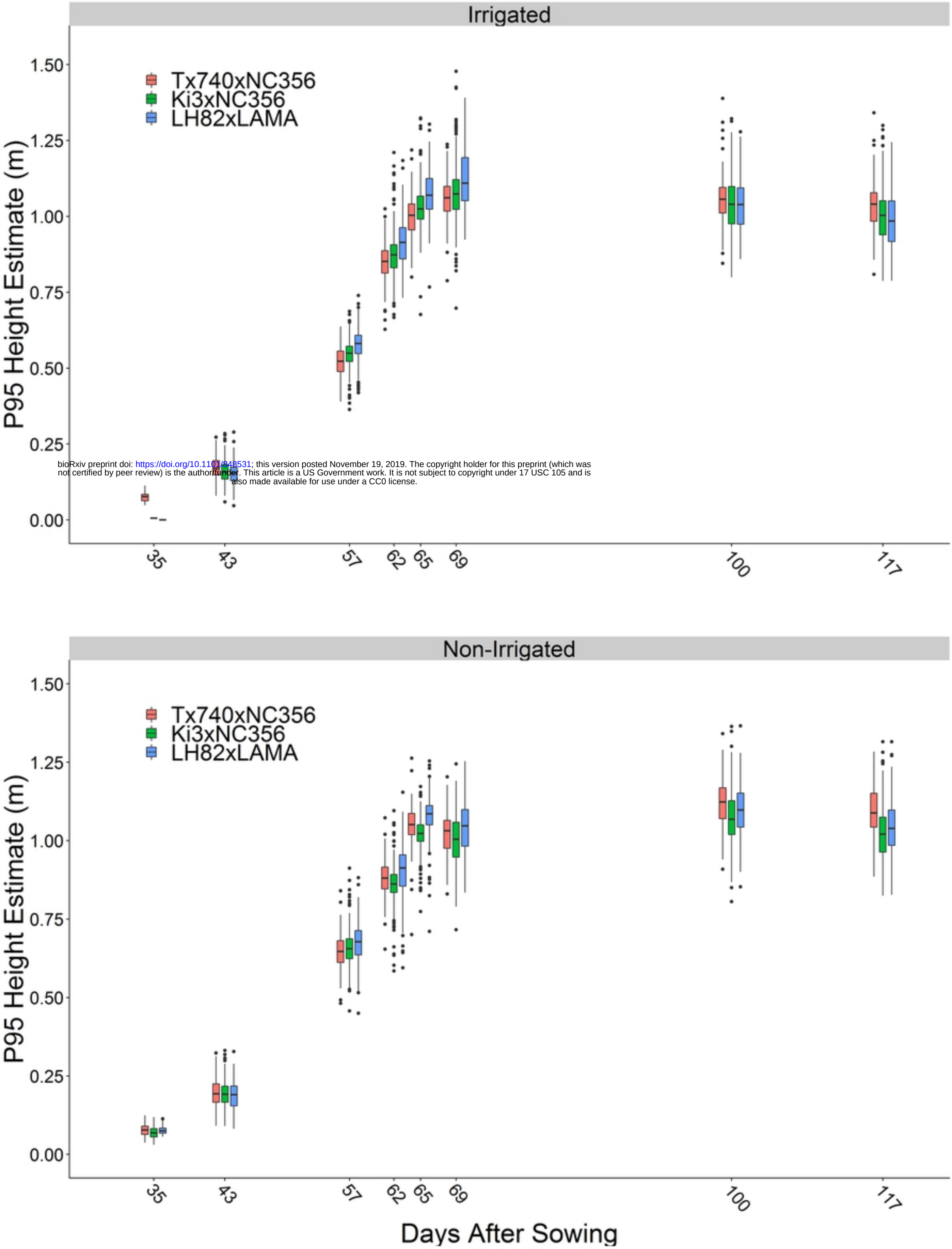

Fig 1

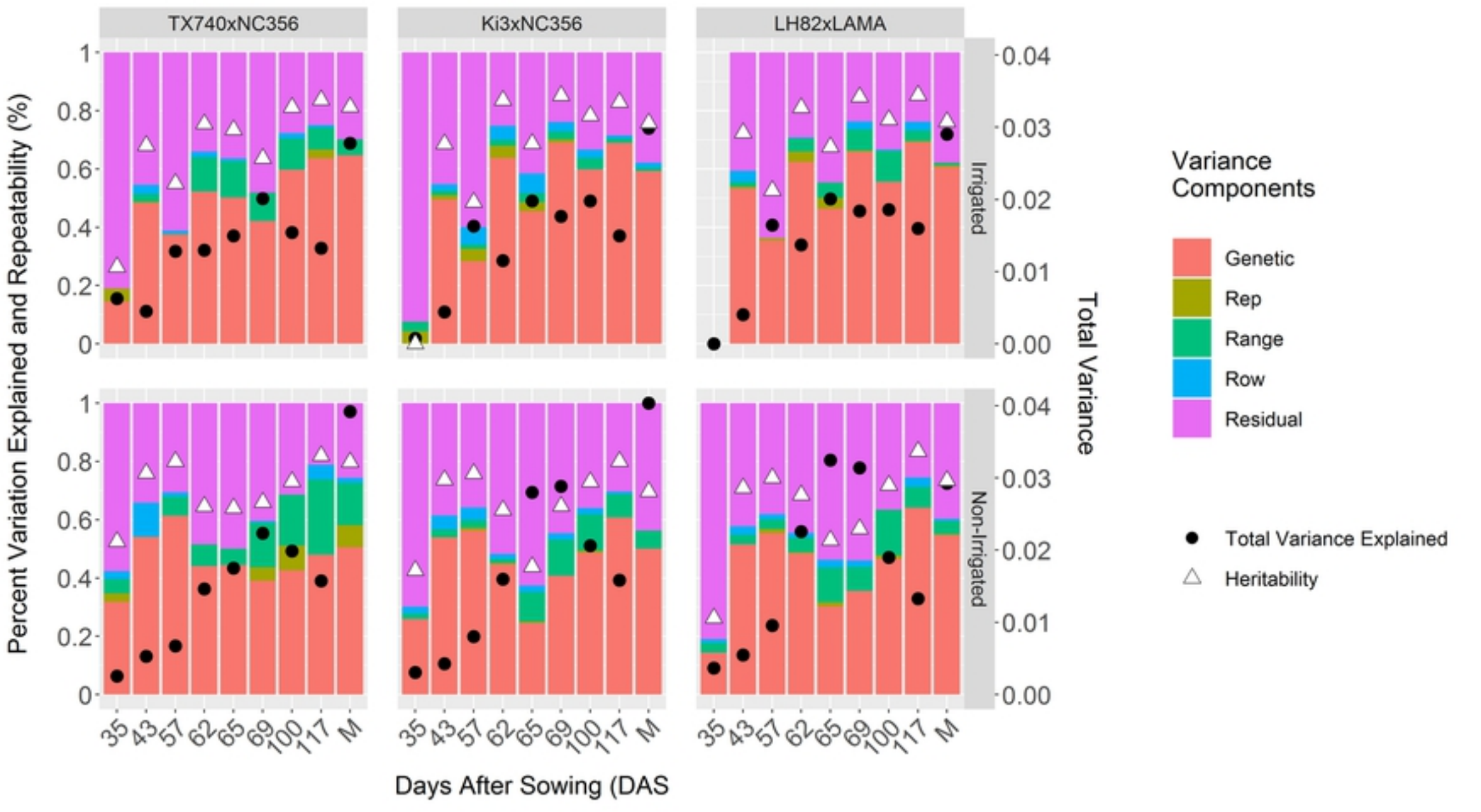
TX740xNC356
Ki3xNC356
LH82xLAMA
Irrigated
Non-Irrigated
Percent Variation Explained and Repeatability (%)
Total Variance
Days After Sowing (DAS
35
43
57
62
65
69
100
117
M
Variance Components
Genetic
Rep
Range
Row
Residual
Total Variance Explained
Heritability

Fig 2

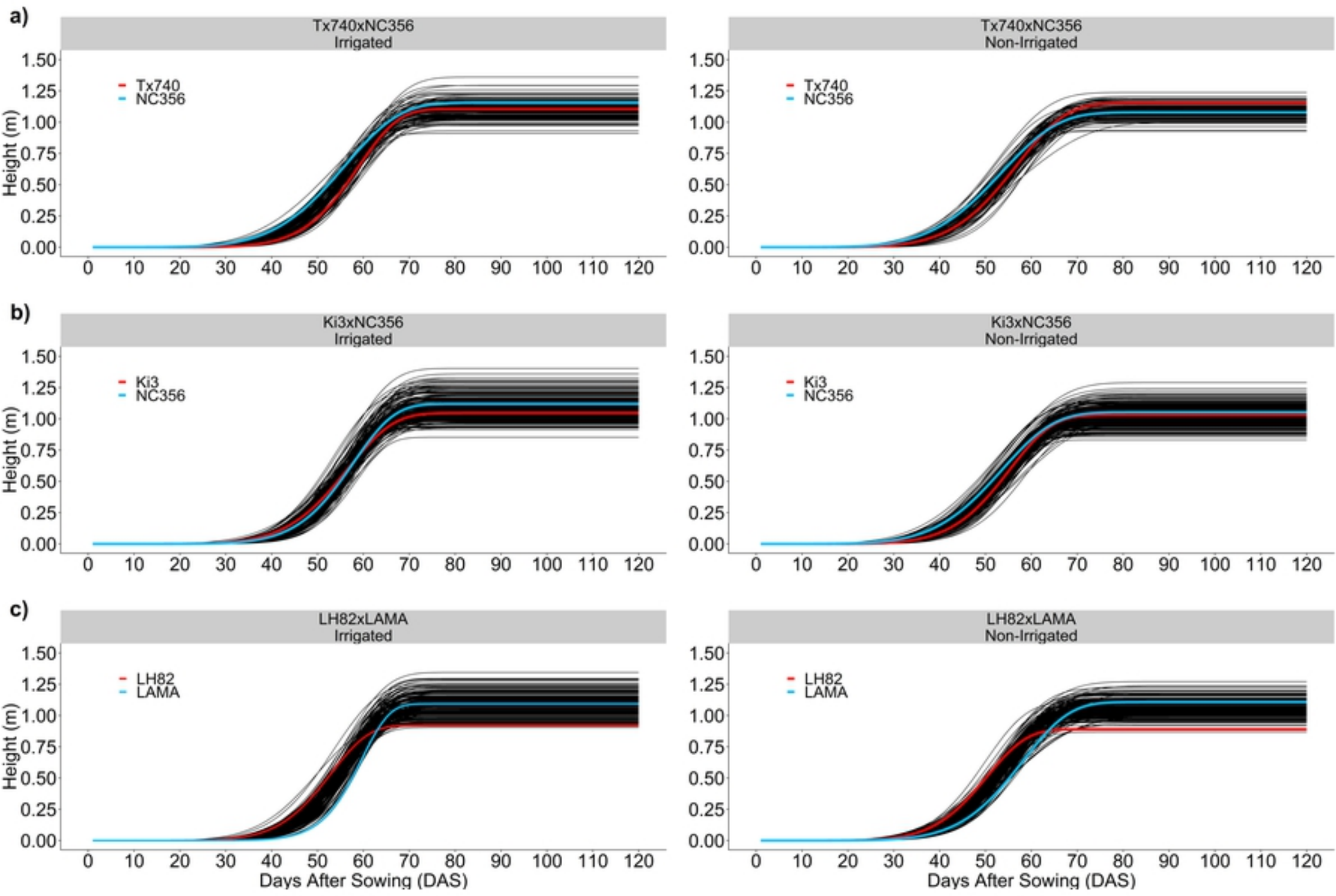
a)
Tx740xNC356
Irrigated
Tx740xNC356
Non-Irrigated
Tx740
NC356
b)
Ki3xNC356
Irrigated
Ki3xNC356
Non-Irrigated
Ki3
NC356
c)
LH82xLAMA
Irrigated
LH82xLAMA
Non-Irrigated
LH82
LAMA
Height (m)
0.00
0.25
0.50
0.75
1.00
1.25
1.50
0 10 20 30 40 50 60 70 80 90 100 110 120
Days After Sowing (DAS)

Fig 3

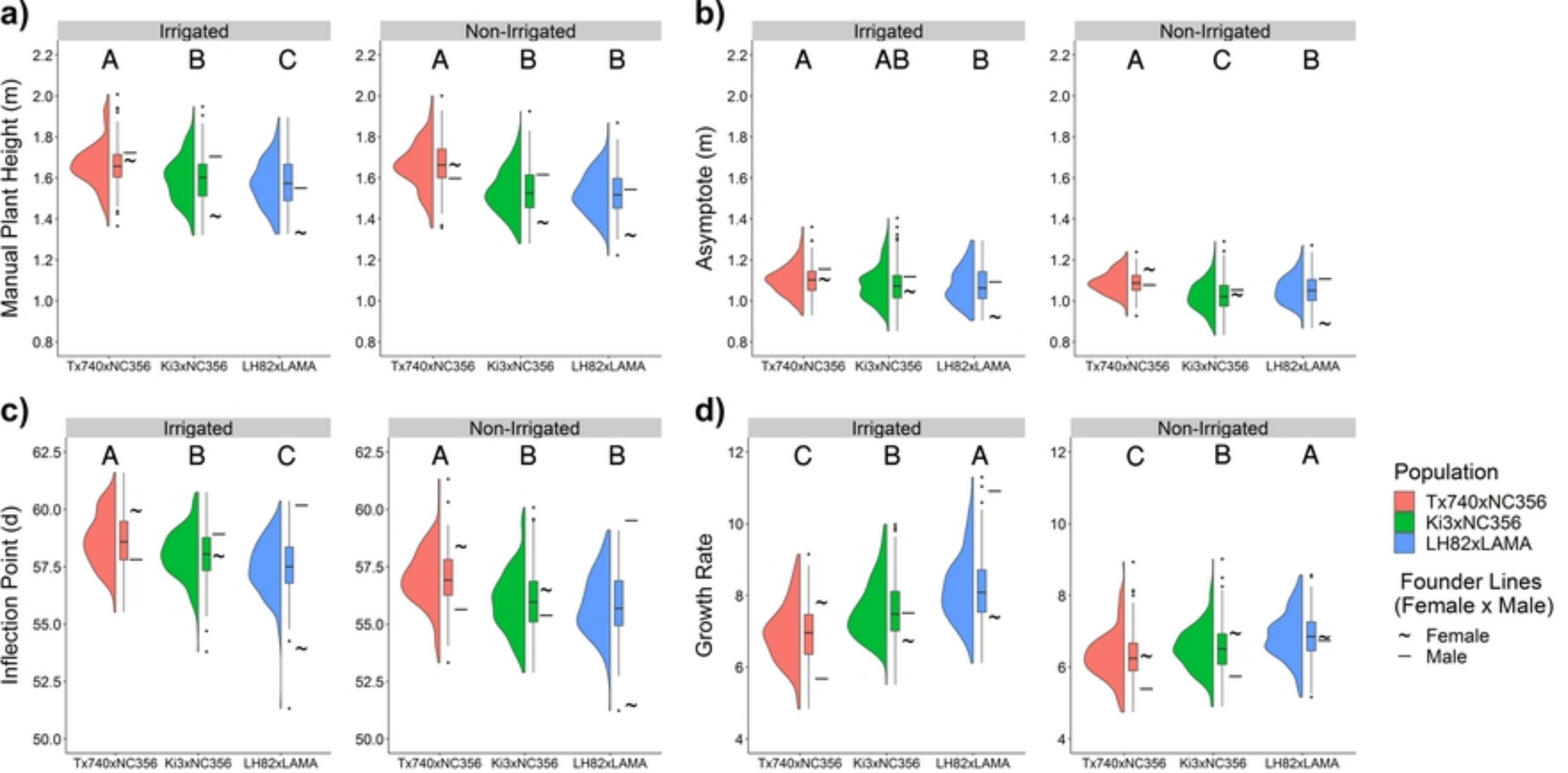
a)
Irrigated
Non-Irrigated
Manual Plant Height (m)
A
B
C
A
B
B
b)
Asymptote (m)
A
AB
B
A
C
B
c)
Inflection Point (d)
d)
Growth Rate
Tx740xNC356
Ki3xNC356
LH82xLAMA
Population
Tx740xNC356
Ki3xNC356
LH82xLAMA
Founder Lines
(Female x Male)
Female
Male

Fig 4

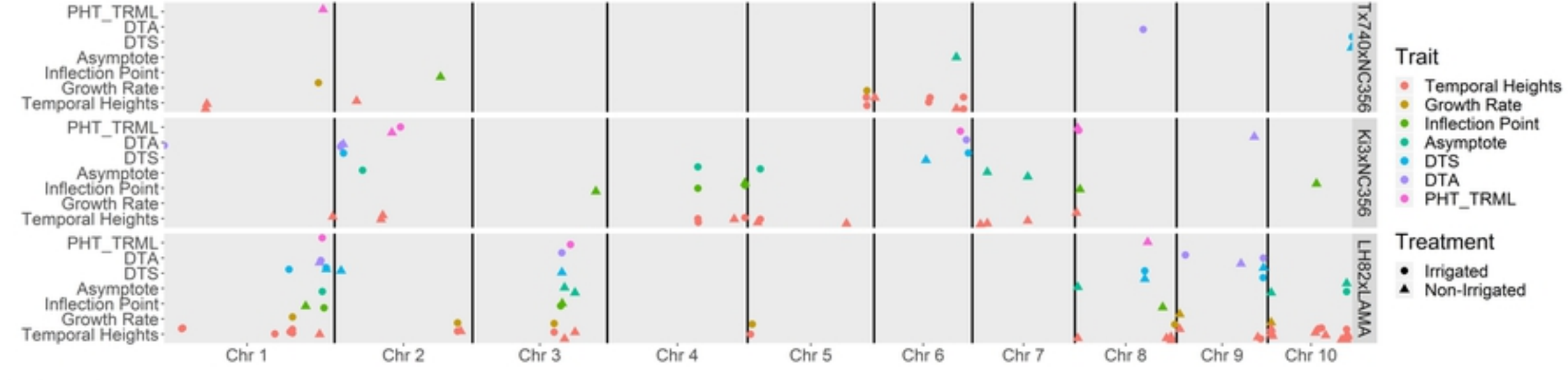
PHT_TRML
DTA
DTS
Asymptote
Inflection Point
Growth Rate
Temporal Heights
Tx740xNC356
Ki3xNC356
LH82xLAMA
Chr 1
Chr 2
Chr 3
Chr 4
Chr 5
Chr 6
Chr 7
Chr 8
Chr 9
Chr 10
Trait
Temporal Heights
Growth Rate
Inflection Point
Asymptote
DTS
DTA
PHT_TRML
Treatment
Irrigated
Non-Irrigated

Fig 5

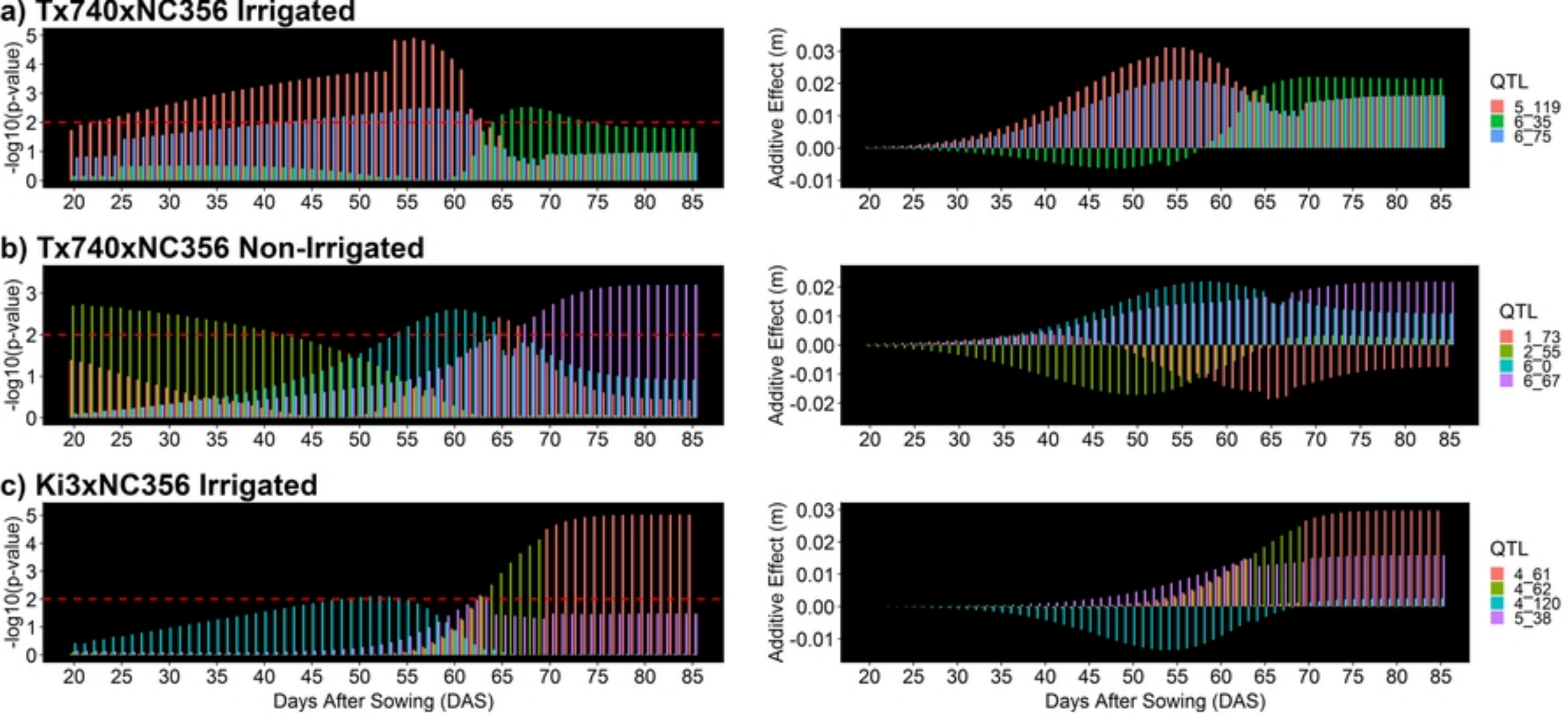
a) Tx740xNC356 Irrigated
b) Tx740xNC356 Non-Irrigated
c) Ki3xNC356 Irrigated
-log10(p-value)
Additive Effect (m)
Days After Sowing (DAS)
QTL
5_119
6_35
6_75
1_73
2_55
6_0
6_67
4_61
4_62
4_120
5_38

Fig 6